Biochemical Engineering Journal 237 (2027) 110440

Contents lists available at ScienceDirect

Biochemical Engineering Journal

journal homepage: www.elsevier.com/locate/bej

Short Communication

Modular microfluidic device for intensified CAR T cell expansion

Jorge Aranda Hernandez [a,1], Oleksandra Derevianko [a,1], Pierre Springuel [a], Pedro Silva Couto [a,2], Jan-Angelus Meyer [b,c], Rainer Krull [b,c], Qasim Rafiq [a], Nicolas Szita [a,*]

[a] Department of Biochemical Engineering, University College London (UCL), Gower Street, London, United Kingdom
[b] Institute of Biochemical Engineering, Technische Universität Braunschweig, Rebenring 56, Braunschweig, Germany
[c] Center of Pharmaceutical Engineering, Technische Universität Braunschweig, Braunschweig, Germany

ARTICLE INFO

Keywords:
CAR T cells
Cell therapy manufacturing
Microfluidics
Perfusion culture
Cell expansion
Modular bioreactor

ABSTRACT

Autologous Chimeric Antigen Receptor (CAR) T cell manufacturing remains costly and labour-intensive, with workflows reliant on manual interventions despite advances in automation. Here, we present a compact microfluidic cell culture device (μCCD) with a simple, modular architecture for intensified CAR T cell expansion. Over four days, the μCCD yielded 10.5×10^8 viable primary T cells compared with 49.8×10^8 viable cells in the G-Rex®, while achieving a 6.7-fold higher viable cell concentration. For CAR T cells, the μCCD achieved a 14-fold expansion, yielding 14.1×10^8 viable cells, compared with 25.1×10^8 viable cells in the G-Rex®, and reaching 56.5×10^6 viable cells·mL^{-1} – a concentration seldom achieved in conventional culture systems and 18-fold higher than a G-Rex® well-based static culture control. Continuous perfusion maintained glucose availability, while integrated oxygen sensors enabled real-time monitoring. Expanded CAR T cells retained cytotoxic activity comparable to G-Rex®-expanded cells under the tested conditions, and microfluidic culture yielded a higher proportion of central memory CAR T cells, which are associated with long-term therapeutic persistence. The platform's modular architecture and low seeding requirement provide a foundation for future clinical-dose manufacturing and rapid assessment of patient-to-patient variability. Together, these results demonstrate the feasibility of the μCCD as a compact and adaptable platform for the high-density expansion of functionally robust CAR T cells. By demonstrating that a modular microfluidic architecture can support the expansion of non-adherent therapeutic cell cultures, this work represents an important step towards more standardised microfluidic platforms for next-generation cell therapy manufacturing.

1. Introduction

Cell and gene therapies represent novel personalised treatments with promising clinical results. Cell-based immunotherapies, in particular, such as the Chimeric Antigen Receptor (CAR) T cell therapy, have demonstrated significant efficacy and durable clinical responses [1]. Since the first approval in 2017, seven CAR T products have been approved by the US Food and Drug Administration (FDA) against acute lymphoblastic leukaemia, non-Hodgkin's lymphoma and multiple myeloma [2]. Despite the clinical success of CAR T immunotherapies, their manufacturing cycle remains labour intensive and time-consuming, leading to high costs per dose (~250,000$) [3] and limiting their widespread clinical use [4].

CAR T manufacturing requires the isolation of white blood cells by leukapheresis, T cell activation, transduction with a Chimeric Antigen Receptor (CAR) transgene and cell expansion. The cell expansion and gene delivery steps are particularly labour-intensive, requiring highly skilled operators [5]. The lack of automation and online monitoring contribute to reduced process control and reproducibility. They also create "open events" that can compromise the product's sterility. To reduce the cost of goods (COG) and manufacturing times, and to improve therapy quality, there is a need for automated manufacturing approaches that eliminate (or minimise) manual operations and the resulting "open events". However, currently available systems are often not fully automated, and their large operating volumes impose high cell seeding numbers, requiring prior manual cell expansions [6,7].

Microfluidic devices are amenable to automation and online sensor integration and are typically closed architectures. Made from polymers,

* Correspondence to: Department of Biochemical Engineering, University College London (UCL), Gower Street, London WC1E 6BT, United Kingdom.
E-mail address: n.szita@ucl.ac.uk (N. Szita).
[1] These authors contributed equally
[2] Current affiliation: Department of Chemical Engineering, University of Bath, Claverton Down, Bath, BA2 7AY, UK

https://doi.org/10.1016/j.bej.2026.110440
Received 28 June 2026; Received in revised form 13 October 2026; Accepted 14 October 2026
Available online 15 October 2026
1369-703X/© 2026 The Authors. Published by Elsevier B.V. This is an open access article under the CC BY license (http://creativecommons.org/licenses/by/4.0/).

they are also amenable as pre-sterilised single-use culture systems. Microfluidics have been applied to different CAR T processing steps with promising results [8,9]. Examples include T cell separation from whole blood [10–14], T cell activation [15,16], integrated lentiviral production [17], automated viral genome engineering [18], enhanced lentiviral transduction [19–21], improved vector potency quantification [22], quality control testing [23], efficacy testing [24], and CAR T cell activation, transduction and expansion in one platform [25], underscoring the great potential of microfluidics for CAR T cell therapies. To fully exploit this potential and accommodate evolving protocols, dose requirements and decentralised manufacturing paradigms, simple and flexible microfluidic systems are required that enable the level of standardisation needed for robust, scalable and well-controlled processing, including effective T cell expansion [26,27].

A modular microfluidic device, originally developed for adherent cell culture and processing [28], has proven versatile for a range of applications. These include m/hESC culture [28,29], transfection [30], hiPSC retinal differentiation [31], and integrated real-time monitoring [29,32–34]. The platform has also been adapted for both cell-free and whole-cell biocatalysis [35]. Given this established versatility and its original design for low shear rates [28], we therefore hypothesised that the platform would also retain non-adherent cells and support the expansion of primary T cells and CAR T cells under controlled culture conditions. If successful, this modular architecture could be readily adapted to different culture volumes, addressing the need for simple, modular and scalable platforms for cell expansion as a key unit operation in cell therapy manufacturing. Furthermore, extending the demonstrated versatility of the platform to include non-adherent therapeutic cell cultures would broaden the range of biological processes supported by the same modular architecture and provide a foundation for the future development of more standardised microfluidic platforms for bioprocessing.

2. Materials and methods

2.1. Lentiviral vector production and titration

A second-generation anti-CD19 CAR lentiviral vector (LV) was produced in HEK293T cells by transient transfection, following the protocol detailed by Costariol et al. [36]. Briefly, the LV preparation encoding the CAR transgene were produced using HEK293T cells (ATCC, US) expanded for 5 days at 5000 cells·cm^{-2}. Cells were transfected with transfer:Gag-Pol:REV:VSVG plasmids at a 4:2:1:1.2 ratio using PEI (Sartorius, Germany) at a DNA:PEI ratio of 1:2.75, following 15 min of complexation at room temperature. Medium was replaced 6 h post-transfection, and supernatants were harvested after 48 h and filtered (0.45 μm). Unless otherwise stated, infectious LV titres were determined using cells seeded at 2×10^6 cells·mL^{-1} in 6-well plates coated with retronectin (4 μg·cm^{-2}). The frozen vector was thawed and titrated using a Jurkat transduction assay.

2.2. T-cell isolation, activation and CAR transduction

Human primary CD3 + T-cells were isolated from a fresh leukopak (BioIVT, West Sussex, UK) on the day of delivery using a Pan T Cell Isolation Kit and LS Columns (Miltenyi Biotec Ltd., UK) as per the manufacturer's instructions. Isolated cells were cryopreserved in CryoStor® CS10 (STEMCELL Technologies UK Ltd, UK) in liquid nitrogen at 5×10^7 cells mL^{-1}. Primary T-cell and CAR T-cell expansion experiments were performed using cells from different donors.

For experiments, cryopreserved T cells were thawed in Rockwell Park Medical Institute (RPMI) medium supplemented with 10% v/v fetal bovine serum, 1% v/v L-glutamine and 1% v/v Antibiotic-Antimycotic (Thermo Fisher Scientific, UK), seeded in static T-flasks (Sarstedt AG & Co. KG, Germany) and incubated at 37°C and 5% CO_2. One day post-thaw, T cells were activated at 1×10^6 cells·mL^{-1} with 1:1 (bead:cell) antiCD3/CD28 Dynabeads™ (Thermo Fisher Scientific, UK) and 30 IU·mL^{-1} research-grade human IL-2 (Miltenyi Biotec Ltd., UK) and incubated overnight. All IL-2 supplementation in this study was performed at this concentration. For primary T-cell expansion experiments, activated T cells were cultured without lentiviral transduction prior to inoculation into the μCCD and G-Rex® vessels. The following day, activated T cells were transduced in 6-well plates (Sarstedt AG & Co. KG, Germany) coated with 4.2 μg·cm^{-2} Retronectin© (Takara Bio Europe, France). LV was added to 1.5×10^6 total cells per well at an MOI of 3, supplemented with IL-2 and spinoculated at 1000 g for 40 min at 32°C, then incubated overnight. One day post transduction, cells were washed, resuspended in fresh IL-2-supplemented medium in T-flasks, and incubated for 48 h prior to inoculation in the 24-well G-Rex® (Wilson Wolf, MN, USA) and the microfluidic cell culture device (μCCD).

2.3. Microfluidic device (μCCD) fabrication

Device parts were designed using Autodesk® Inventor software and converted to G-code with Autodesk® HSM Express™ for a 3-axis milling machine (CNC Mini-Mill, Minitech®, USA). Micro-milling fabricated the three cycloolefin polymer (COP) device layers and PDMS casting moulds. Contour milling created cut-through features (e.g. device edges, culture chambers), while pocket milling formed depth-defined features (e.g., channels). Lateral side-channels (1.4 mm × 0.5 mm) were incorporated to facilitate cell seeding and harvesting. The device was assembled via thermo-compression bonding (150 °C, 1.25 h). T-shaped PDMS lids were fabricated by casting and curing at 80 °C for 120 min.

2.4. Cell seeding, expansion, counting, and viability assays

All parts of the μCCD were autoclaved. Device assembly and cell seeding were performed in a laminar flow hood to maintain sterility. The μCCD was connected to syringes using 1/16" poly-ether-ether-ketone (PEEK) tubing and metric chromatography connectors (Thermofisher Scientific, UK). Primary T cells and CAR T cells were expanded using the same seeding densities, but with slightly different perfusion schedules, as detailed below. Inoculation in μCCD and 24-well G-Rex® occurred two days after subculture. Prior to inoculation, cell suspension concentrations were adjusted to achieve the same cell seeding density of 0.5×10^6 cells·cm^{-2} in both devices. The μCCDs were inoculated with 250 μL of cell suspension; and the G-Rex® wells were inoculated with 250 μL cell suspension supplemented with 7.75 mL of completed RPMI media.

For CAR T cell expansion, microfluidic cultures were perfused (PHD Ultra, Harvard Apparatus) at flow rates of 5 μL min^{-1} on day 1, 7.5 μL min^{-1} on day 2, and 10 μL min^{-1} for the final 2 days. For primary T-cell expansion, the flow rate was maintained at 5 μL·min^{-1} for the first two days and increased to 10 μL·min^{-1} for the final two days. On day 2, syringes containing fresh media and IL-2 were exchanged. G-Rex® vessels were spiked with IL-2, and 6 mL of fresh medium exchanged after 2 days. All cultures were maintained in a CO_2 incubator at 37 °C with 5% CO_2.

At the end of the experiments, perfusion in the μCCDs was halted and tubing disconnected from syringe pumps. Devices were transferred from incubator to a laminar flow hood for cell recovery and quantification. To aid cell recovery and empty the culture chamber, metric plugs (P-314, Idex) were used to restrict flow in the perfusion channels. The culture chamber was washed with pre-heated PBS (Gibco, Thermo Fisher Scientific). The resulting volumes from sequential rinsing were pooled for each device. Cell counts and viability were measured at inoculation and recovery with a NucleoCounter® NC-3000™ with Via-1-Cassettes™ (ChemoMetec A/S©, Denmark). G-Rex® cultures were harvested manually according to the manufacturer's instructions. Total viable cell yields were calculated from the measured viable cell concentrations and corresponding harvest volumes. For the G-Rex®, reported viable cell concentrations were calculated by dividing the total viable cell yield by

the 8 mL working culture volume.

2.5. Flow cytometry

Phenotypic characterisation of CAR T cells was performed using a LSRFortessa X-20 flow cytometer (BD Biosciences, UK). Cells viability was assessed with LIVE/DEAD Fixable Violet Dead Cell Stain kit (Thermo Fisher Scientific, UK), followed by surface staining for CD3-BUV395, CD4-BUV805, CD8- APC-Cy7, CCR7-BV421, CD45RO-PE-Cy7 (BD Biosciences, UK), CD34(CAR)-AlexaFluor647 (Bio-Techne Ltd., UK), PD-1-PE, and LAG-3- BV711 (BioLegend, UK) antibodies. The gating strategy used for flow cytometric analysis is summarised in Supplementary Figure S1.

2.6. CAR T cytotoxicity assay

CAR T cells were purified using a CD34 MicroBead Kit and LS Columns (Miltenyi Biotec Ltd., UK) [37]. Purified CAR T cells were co-cultured at a 1:1 (CAR-T cell: target cell) ratio with GFP +, CD19 + NALM6 target cells in poly-L-lysine-coated 96-well plates (Sigma Aldrich Merck, UK; Sarstedt AG & Co. KG, Germany). Fluorescence was monitored for 48 h using an Incucyte® S3 Live-Cell Analysis System (Sartorius, UK) to assess cytotoxicity.

2.7. Monitoring of dissolved oxygen in μCCD

Optical oxygen sensors (PyroScience GmbH, Aachen, Germany) were integrated into the μCCD during fabrication, with one sensor in the inlet channel (upstream of the culture chamber) and one in the outlet channel (downstream). Sensors were read out in real-time using a FireSting O2 optical oxygen meter controller (PyroScience GmbH, Aachen, Germany). The outlet sensor value was calculated by assuming 100% air saturation at the inlet and then subtracting the measured difference between the inlet and outlet sensors.

2.8. Monitoring of glucose in cultures

Glucose concentrations in the culture medium were measured offline using a Contour® Next One Blood Glucose Meter and disposable test strips (Ascensia Diabetes Care UK Ltd., England). For the perfused μCCD, samples were taken from the collected effluent. For the G-Rex® system, samples were taken from the discarded medium following media exchanges. The final glucose concentration was calculated by subtracting the known baseline concentration of the RPMI medium from the measured value.

2.9. Data analysis

Data was analysed and visualised using GraphPad Prism. Statistical significance was assessed using one way ANOVA and Tukey's multiple comparison test.

3. Results

Similar to previous designs [22,30,31], the microfluidic cell culture device (μCCD) featured a rectangular culture chamber sealed by a re-sealable 'T-shaped' lid (Fig. 1, Fig. S2). Flow distributors on each side of the chamber created a uniform fluid flow velocity profile. Media entered *via* a single inlet channel, passed through distributor and culture chamber, and exited *via* distributor through a single outlet channel. In the present implementation, the 'T-shaped' lid was made from polydimethylsiloxane (PDMS) to enhance oxygenation, while the main device body was fabricated from three cyclo-olefin polymer (COP) layers. To increase cell capacity, the culture chamber's surface area and depth were enlarged compared to earlier models [22,30,31], resulting in a volume of 270 μL (26 mm × 8 mm × 1.3 mm). Cells were loaded through lateral side channels (1.4 mm × 0.5 mm), positioned on the short sides of the chamber. Retention within the culture chamber under perfusion was evaluated using 10 μm fluorescent particles as a cell-sized model (Fig. S3).

Primary T-cell and CAR T-cell expansion experiments were performed in parallel in μCCDs and benchmarked against gas-permeable G-Rex® wells. To facilitate comparison, the inoculation cell number was selected at the lower limit of the G-Rex® manufacturer's recommendation to accommodate the μCCDs' much smaller volumes (270 μL *vs* 8 mL). Both systems were inoculated with one million cells only. Since each system has a surface area of 2 cm^2, this resulted in an identical seeding density of 0.5 × 10^6 cells·cm^{-2} (Fig. 2).

For primary T cells, after four days of expansion, the average number of viable cells was 10.5 × 10^6 (± 4.95 ×10^5 cells) in the μCCDs and 49.8 × 10^6 (± 7.26 ×10^6 cells) in the G-Rex® wells (Fig. 2A). This resulted in an average viable cell concentration of 41.9 × 10^6 cells·mL^{-1} (± 1.98 ×10^6 cells·mL^{-1}) in the μCCDs, compared with 6.22 × 10^6 cells·mL^{-1} (± 9.07 ×10^5 cells·mL^{-1}) in the G-Rex® vessels (Fig. 2B). Cell viability averaged 92.45% (± 2.33%) in the μCCDs, compared with 95.6% (± 1.02%) in the G-Rex® (Fig. 2C).

For CAR T cells, after four days of expansion, the average number of viable cells was 14.1 × 10^6 (± 2.14 ×10^6 cells) in the μCCDs and 25.1 × 10^6 (± 1.67 ×10^6 cells) in the three G-Rex® wells (Fig. 2D). This resulted in an average viable cell concentration 56.5 × 10^6 cells·mL^{-1} (± 8 ×10^6 cells·mL^{-1}) in the μCCDs, which was significantly higher than

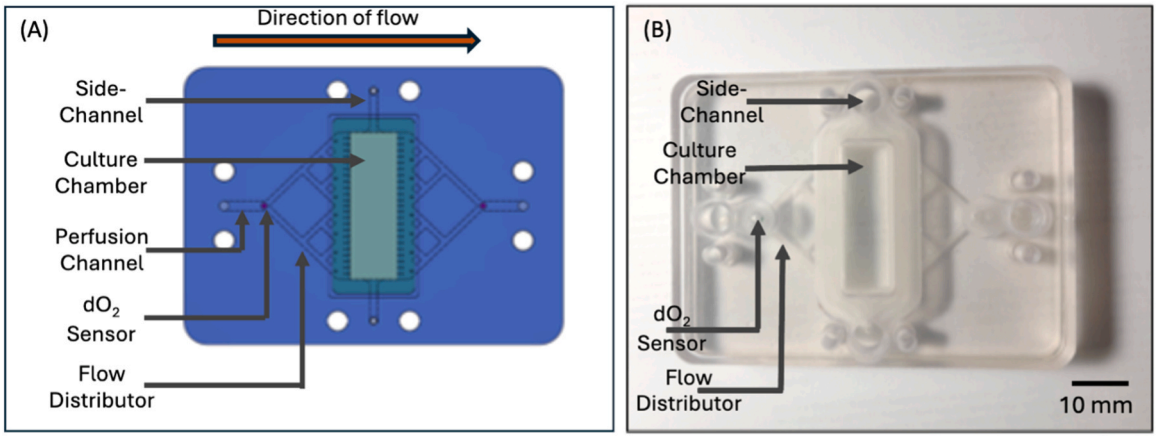


Fig. 1. Schematic representation (A) and photograph (B) of the microfluidic cell culture device (μCCD). CAR T cells were cultured in the culture chamber (26 mm × 8 mm × 1.3 mm). Culture media was perfused into the chamber via flow distributors channels up- and downstream of the chamber. Lateral side channels (1.4 mm × 0.2 mm) were employed for cell seeding and harvest. A T-shaped lid, made from gas-permeable PDMS to facilitate cell oxygenation, enclosed the chamber.

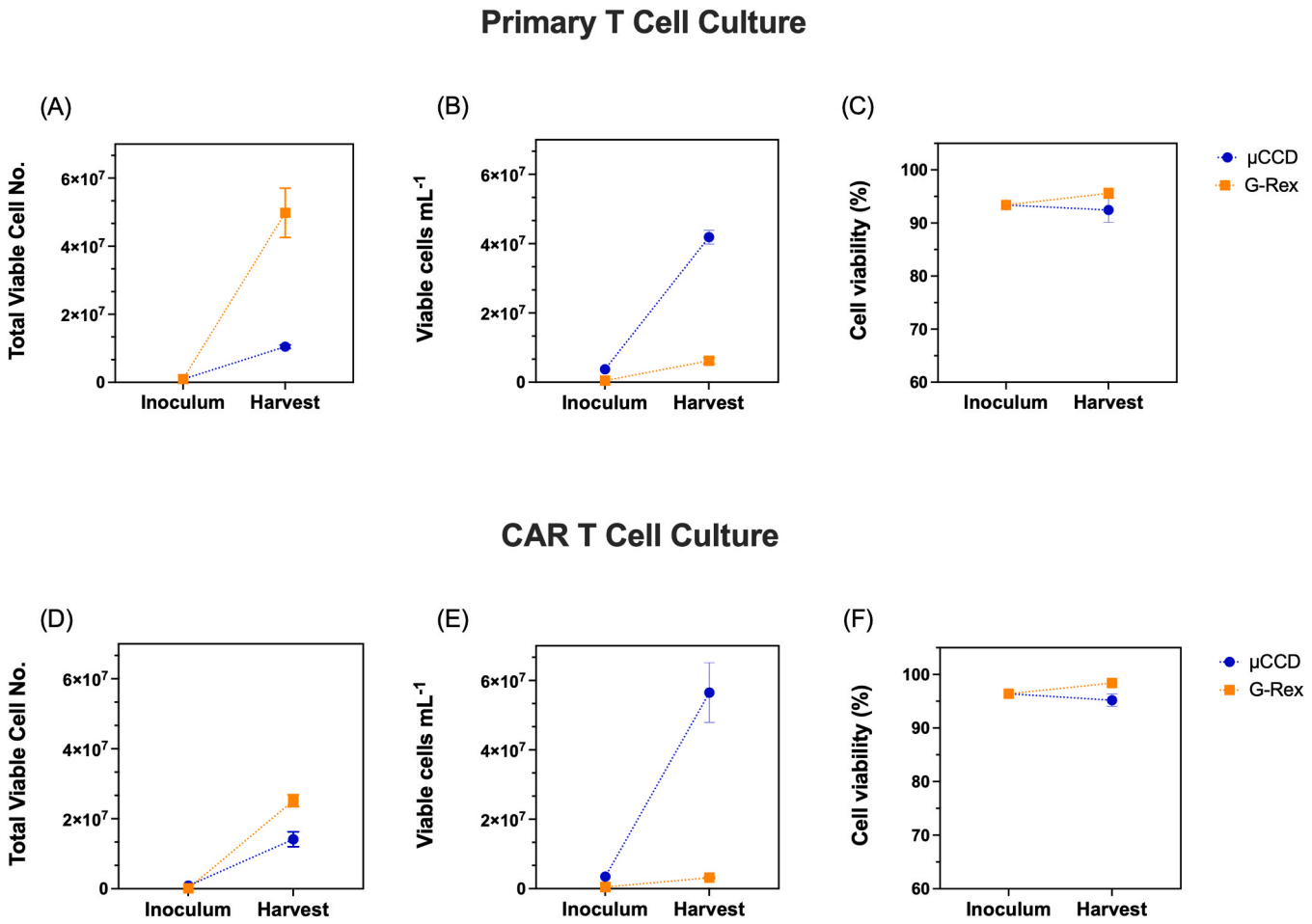


Fig. 2. Primary T-cell and CAR T-cell expansion over four days in the μCCDs (blue) and G-Rex® vessels (amber), from inoculum to harvest. (A–C) Primary T-cell expansion: (A) total viable cells at harvest for the μCCDs ($10.5 \times 10^6 \pm 0.495 \times 10^6$ cells) and G-Rex® vessels ($49.8 \times 10^6 \pm 7.26 \times 10^6$ cells); (B) viable cell concentration at harvest for the μCCDs ($41.9 \times 10^6 \pm 1.98 \times 10^6$ cells·mL^{-1}) and G-Rex® vessels ($6.22 \times 10^6 \pm 0.907 \times 10^6$ cells·mL^{-1}); (C) cell viability at harvest for the μCCDs (92.45 ± 2.33%) and G-Rex® vessels (95.6 ± 1.02%). (D–F) CAR T-cell expansion: (D) total viable cells at harvest for the μCCDs ($14.1 \times 10^6 \pm 2.14 \times 10^6$ cells) and G-Rex® vessels ($25.1 \times 10^6 \pm 1.67 \times 10^6$ cells); (E) viable cell concentration at harvest for the μCCDs ($56.5 \times 10^6 \pm 8 \times 10^6$ cells·mL^{-1}) and G-Rex® vessels ($3.14 \times 10^6 \pm 0.2 \times 10^6$ cells·mL^{-1}); (F) cell viability at harvest for the μCCDs (95.2 ± 1.15%) and G-Rex® vessels (98.4 ± 0.173%). Data are expressed as mean ± SD (n = 2 per group for primary T cells; n = 3 per group for CAR T cells), with technical replicates from a single donor for each cell type.

the 3.14×10^6 cells·mL^{-1} ($\pm 0.2 \times 10^6$ cells·mL^{-1}) in the G-Rex® vessels (Fig. 2E) – a concentration 18-fold higher than in the G-Rex®. Cell viability averaged 95.2% (± 1.15%) in the μCCDs, compared with 98.4% (± 0.17%) in the G-Rex® (Fig. 2F).

Offline glucose measurements (Fig. S4) revealed that the concentration in the μCCD decreased during the first two days of culture from 11.1 mM to 8.0 mM, then stabilised until harvest on day 4. In contrast, while a comparable glucose concentration of 7.9 mM was measured in the G-Rex® vessels on day 2, it decayed to 5.8 mM by day 4. The perfusion regime in the μCCD maintained glucose levels above 70% of the initial medium concentration throughout the culture, whereas approximately 52% remained at the end of the G-Rex® cultures. A similar trend was observed during primary T-cell expansion, with glucose concentrations of 8.91 mM (80% of the initial concentration) in the μCCD and 5.03 mM (45%) in the G-Rex® after four days of culture.

In terms of resource use, the perfusion-based μCCD consumed more than three times as much medium as the G-Rex®, requiring 46.8 mL per device compared with 14 mL per G-Rex® well over the four-day CAR T cell cultures (43.2 mL for primary T-cell expansion in the μCCD). Normalising medium consumption to the viable cell number at harvest, the μCCD required 3.3 mL per 10^6 viable CAR T cells (4.1 mL per 10^6 primary T cells), compared with 0.56 mL per 10^6 viable CAR T cells (0.28 mL per 10^6 primary T cells) for the G-Rex® (Table 1). Medium consumption in the μCCD was not optimised, and the limited glucose depletion observed during culture suggests that lower perfusion rates may be feasible without compromising cell growth.

Table 1
Viable cell yield and medium-use efficiency for primary T-cell and CAR T-cell expansion in the μCCD and G-Rex® systems.

Cell type	μCCD (mL per 10^6 viable cells)	G-Rex® (mL per 10^6 viable cells)
Primary T cells	4.1	0.28 mL
CAR T cells	3.3	0.56 mL

Dissolved oxygen (DO) was monitored in real time using optical sensors integrated in the inlet and outlet channels of the device, with measurements taken every hour. As shown in Fig. 3, for the CAR T cells, outlet DO levels decreased from full air saturation to 39% air over the four-day culture period, indicating cell growth and oxygen consumption. Spikes observed at the 24- and 48-hour marks correspond to increases in media flow rate; these scheduled increases in flow rate were intended to slow the rate of DO depletion within the culture chamber. The DO level at the outlet continued to decrease (albeit more slowly), suggesting that the cells remained in their expansion phase and could be

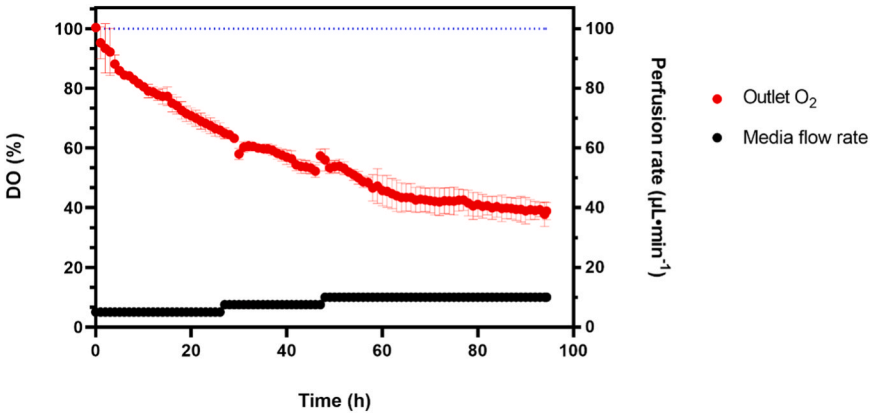


Fig. 3. Real-time oxygen monitoring using optical sensors integrated in the µCCDs. During a 4-day CAR-T cell culture, average outlet dissolved oxygen (DO) saturation decreased from 100% to 39% (red dots, left ordinate axis). The perfusion flow rate (black dots, right ordinate axis) was stepwise increased from 5 µL min^{-1} (day 1) to 7.5 µL min^{-1} (day 2), and to 10 µL min^{-1} (days 3 and 4). The blue dashed line represents inlet DO, normalised to 100% air saturation; outlet DO data was normalised against the inlet data. All data are expressed as mean ± SD of triplicate devices from a single experiment.

cultured in the µCCD for a longer duration. A similar decrease in outlet DO was observed during primary T-cell expansion.

Phenotypic characterisation of CAR T cells was performed by flow cytometry at inoculation and after four days of culture, in both µCCD and G-Rex® (Fig. 4). At inoculation, 73.9% (± 0.058%) of cells expressed the CAR gene expression. After culture, this fraction decreased to 65.6 ± 1.20% in the µCCD and 63.8% (± 1.10%) in the G-Rex® (Fig. 4A); this difference was not statistically significant. The CD4 + / CD8 + ratio decreased significantly in both expansion platforms, with a slightly more pronounced decrease in the G-Rex® (ratio of 1.7 ± 0.098) than in the µCCD (ratio of 1.9 ± 0.013) (Fig. 4B).

Analysis of exhaustion markers revealed that PD-1 and LAG-3 expression on CD3 + T cells decreased during expansion, from 96.7% (± 0.321%) in the inoculum to 43.2% (± 1.39%) in the µCCD and 33.2% (± 1.29%) in the G-Rex® (Fig. 4C). The high initial expression of these markers was likely due to the ex vivo pre-expansion and activation steps of the T cells; their subsequent decrease is consistent with active cell proliferation and the increased cell concentrations observed at harvest. The difference in PD-1/LAG-3 expression between the µCCD and G-Rex® at harvest was statistically significant.

Analysis of CD8 + T cell subpopulations was performed to determine the percentages of central memory, effector memory, and terminally differentiated cells (Fig. 4D-4F). During the expansion, both G-Rex® and µCCD showed a statistically significant increase in effector cells, though the percentage was slightly higher in the G-Rex® (>0.075%) than in the µCCD (~0.05%). Post-harvest, cells grown in in the µCCD expressed significantly fewer effector memory markers, which could potentially delay tumour cell killing. However, µCCD-grown cell exhibited significantly higher levels of central memory markers than those from the G-Rex®.

The functional capacity of the CAR T cells was evaluated using an *in vitro* cytotoxicity assay with fluorescent CD19 + NALM6 target cells. As shown in Fig. 5, CAR T cells from both systems were highly functional, demonstrating potent cytotoxicity. Under the tested 1:1 effector-to-target ratio, CAR T cells expanded in both the µCCD and G-Rex® demonstrated potent cytotoxic activity. Indeed, after 24 h of co-culture, NALM6 target cells were nearly eliminated in both groups, indicating that the assay reached near-maximal target cell killing under the conditions tested.

4. Discussion

This study successfully demonstrated the expansion of both primary T cells and CAR-T cells in a perfused microfluidic platform (µCCD), achieving markedly higher viable cell concentrations than a conventional G-Rex® system. For the CAR T cells, the µCCD reached a viable concentration of 56.5 × 10^6 cells·mL^{-1} compared to 3.14 × 10^6 cells·mL^{-1} , a density rarely reported and underscoring this approach for process intensification [25,38]. A similar increase in viable cell concentration was observed for primary T cells, reaching 41.9 × 10^6 cells·mL^{-1} in the µCCD compared with 6.22 × 10^6 cells·mL^{-1} in the G-Rex®. However, both primary T-cell and CAR T-cell cultures yielded fewer total viable cells in the µCCD than in the G-Rex®, highlighting the distinction between high volumetric cell concentration and absolute cell yield. The higher viable cell concentrations in the µCCD may be partly attributable to improved nutrient availability under continuous perfusion, as suggested by the relatively stable glucose concentrations compared with the depletion observed in the G-Rex® system.

Beyond high volumetric productivity, the µCCD also enabled continuous monitoring of the culture environment. The integrated in-line dissolved oxygen (DO) sensors provided real-time insight into cellular respiration and increasing oxygen demand throughout CAR T cell expansion, allowing perfusion rates to be adjusted in response to the observed metabolic activity of the culture. Such continuous process monitoring is not readily achievable in conventional static G-Rex® cultures without disruptive sampling. Offline glucose measurements further indicated that the applied perfusion strategy maintained nutrient availability throughout both primary T cell and CAR T cell cultures, in contrast to the progressive depletion observed in the G-Rex® system. Together, these results demonstrate the potential of integrated sensing within microfluidic platforms and provide a foundation for future implementation of more comprehensive process analytical technology (PAT).

From a process performance perspective, the device demonstrated competitive CAR T cell expansion from a low seeding number (~1 × 10^6 cells). This is a key advantage given the high cost and limited availability of patient-derived cells from leukapheresis, reducing reagent consumption and pressure on pre-expansion steps, particularly for heavily pre-treated patients [36]. Beyond high-density manufacturing, the small volume and parallelisation opportunity of the µCCD make it well suited for early-stage process development. Although the present study did not investigate donor-to-donor variability, the significant variability in T cell proliferation between patients necessitates rapid optimisation of activation, transduction and expansion strategies. The µCCD could therefore facilitate future evaluation of donor-specific expansion strategies using limited numbers of cells. Diseased or senescent T cells, for example, may require specialised expansion strategies which could be quickly tested with a few microfluidic devices capable of operating with a small number of cells.

Based on the CAR T cell yields obtained in this study, approximately

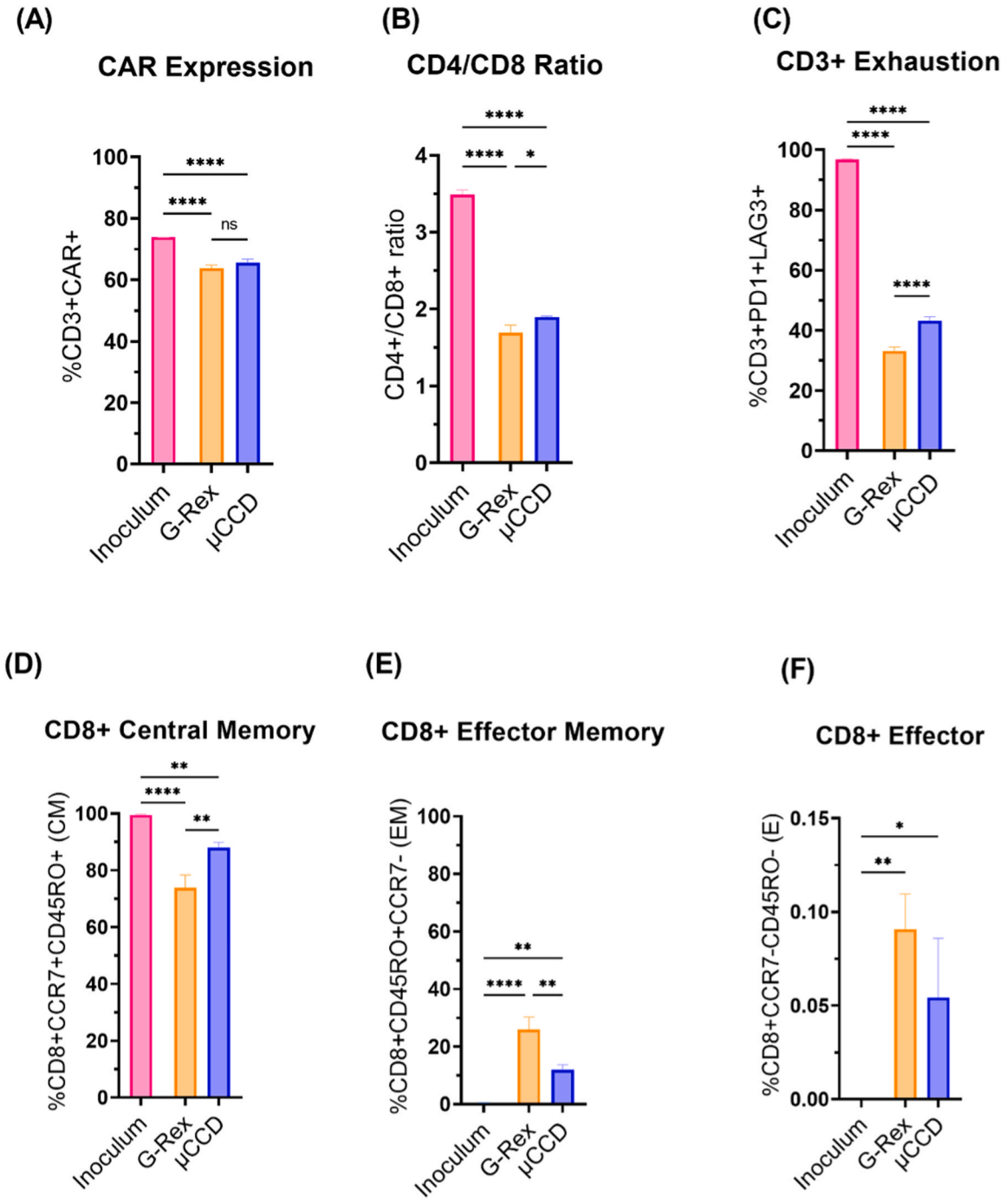


Fig. 4. Phenotypic characterisation of primary T cells in G-Rex® well plates and the µCCDs at inoculation and after harvest. (A) Percentage of viable cells expressing the CAR marker. (B) CD4 + /CD8 + T cell. (C) Percentage of total live cells expressing exhaustion markers PD-1 and LAG-3. (D) Percentage of CD8 + T central memory (CCR7 + CD45RO+) cells. (E) Percentage of CD8 + T effector memory (CCR7- CD45RO+) cells. (F) Percentage of CD8 + T effector (CCR7- CD45RO-) cells. All data is expressed as mean ± SD (n = 3 per group) from a single experiment. Significance was assessed using one way ANOVA and Tukey's multiple comparison test (ns: $p > 0.05$; *: $p < 0.05$; **: $p < 0.01$; **** $p < 0.0001$).

15 devices would be required for a therapeutic dose (200–250 million cells). In contrast, larger G-Rex® formats, such as the G-Rex®100, can achieve substantially higher absolute cell yields, highlighting the current limitation of the µCCD for production-scale expansion. However, continuous perfusion of the µCCD enables frequent medium replenishment while retaining cells within a small culture volume, which may contribute to the higher viable cell concentrations observed compared with the G-Rex® control. Scaling can be achieved not only by parallelisation - which presents engineering challenges - but by increasing the yield from a single device. This approach is supported by our previous work with the device's modular architecture, which was successfully scaled up for biocatalysis applications [35]. In addition to enlarging the culture chamber, future iterations will focus on extending expansion times and optimising perfusion rates, potentially using a closed-loop feedback system based on the platform's integrated dissolved oxygen (DO) sensors to maximise growth rates and final cell yield. The modular architecture also provides a straightforward route to integrating additional sensing modalities, such as glucose or lactate sensors, as well as

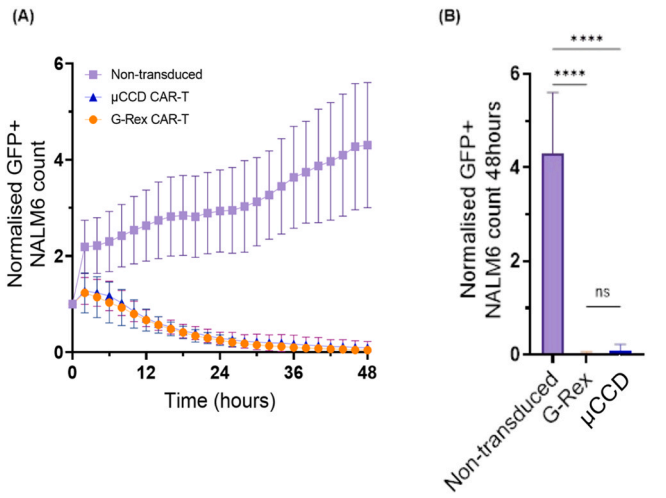


Fig. 5. Functional characterisation of CAR T cells via killing assay, showing comparable functionality between cells from μCCDs and the G-Rex® wells. (A) NALM6 cell counts over 48-hour killing assay, measured every 2 h, for target cells alone, target cells co-cultured with μCCD-grown CAR T cells, and target cells co-cultured with G-Rex®-grown CAR T cells. (B) Remaining NALM6 target cell count after the 48-hour functionality assay. All data is expressed as mean ± SD (n = 3 per group) from a single experiment. Significance was assessed using one way ANOVA and Tukey's multiple comparison test (ns: $p > 0.05$; **** $p < 0.0001$).

model-based soft sensors, enabling more sophisticated multi-parameter process monitoring and control without substantial modifications to the device.

Despite these advantages, challenges remain. The μCCD also consumed more than three times the medium volume of the G-Rex® during the four-day culture, which would represent an important cost consideration for manufacturing. However, medium consumption was not optimised in this proof-of-concept study. The maintenance of glucose concentrations at approximately 8 mM from day 2 to day 4 in both primary and CAR T cell expansion suggests that lower perfusion rates may be feasible, and optimisation of medium delivery should therefore form part of future process development. Additionally, CAR T cell expansion in the μCCD (14-fold) was lower than that achieved with the G-Rex® (25-fold) expansion, and the increased variability suggests that process robustness remains to be improved. This variability may partly reflect fabrication tolerances that introduce variations in chamber geometry, resulting in differences in flow distribution and local mass transfer within the microscale culture environment, highlighting a key engineering challenge for scaling out.

CAR T cell phenotypic analysis revealed a complex trade-off: while the μCCD showed a higher proportion of desirable central memory T cells, it also retained a slightly higher proportion of PD-1/LAG-3-positive cells from the inoculum (43.2% vs. 33.2%), indicating persistence of activation-induced exhaustion markers. The key challenge is therefore to optimise the culture conditions to balance high-density expansion with the preservation of a favourable therapeutic phenotype. A further limitation of this initial feasibility study is that primary T-cell and CAR T-cell expansion were each evaluated using cells from a single, different donor, and under slightly different perfusion schedules. Consequently, differences in expansion performance between the two cell types cannot be attributed specifically to CAR transduction. While technical replicates provided an initial assessment of device performance under identical culture conditions, the findings require confirmation using additional independent donors to establish biological reproducibility, assess donor-to-donor variability, and further evaluate the robustness and generalisability of the platform.

Despite these limitations, the functional killing assay demonstrated that CAR T cells expanded in both systems retained potent cytotoxic activity under the tested 1:1 effector-to-target conditions. These findings indicate that the μCCD not only supports high-density culture but also maintains CAR T cell cytotoxic function. Because the 1:1 effector-to-target ratio resulted in near-complete target cell elimination, more subtle differences in cytotoxic potency between the two culture systems may not have been resolved. Future studies should therefore evaluate additional effector-to-target ratios to provide a more stringent functional comparison. More broadly, the platform's closed, single-use nature could support a shift from centralised to decentralised point-of-care manufacturing, reducing costs and treatment delays. While the present study focused specifically on the CAR T cell expansion stage, integration of the μCCD with upstream operations, including T cell activation and transduction, represents an important next step towards a more complete manufacturing workflow.

Finally, the modular architecture of the μCCD directly addresses the need for simple, modular and flexible systems that can support standardisation across cell therapy manufacturing. The μCCD uses a relatively simple architecture based on a single perfused culture chamber, in contrast to microfluidic approaches integrating multiple CAR T processing operations within a single device [25]. Other microfluidic systems for non-adherent T cell culture have employed membrane-separated culture and perfusion compartments [39], whereas the μCCD retains cells directly within the perfused culture chamber. Its simplicity is demonstrated by the ease with which the culture chamber can be enlarged to increase yield, as previously shown [35]. Importantly, its flexibility is demonstrated by the successful application of the same underlying platform architecture across a diverse range of biological domains—from adherent and non-adherent human cell cultures to cell-free and whole-cell biocatalysis—without requiring application-specific device redesign. This growing body of evidence for the versatility of a single modular architecture represents an important step towards more standardised microfluidic platforms for bioprocessing. By providing a consistent, well-characterised platform that can be adapted for multiple processes, the μCCD represents a promising platform for further development towards robust and scalable manufacturing processes of next-generation cell therapies.

CRediT authorship contribution statement

Jorge Aranda Hernandez: Writing – original draft, Validation, Methodology, Investigation, Formal analysis, Data curation, Conceptualization. **Oleksandra Derevianko:** Writing – review & editing, Writing – original draft, Investigation, Formal analysis, Data curation. **Pierre Springuel:** Writing – original draft, Resources, Investigation, Formal analysis. **Pedro Silva Couto:** Data curation, Writing – review & editing. **Jan-Angelus Meyer:** Investigation. **Rainer Krull:** Writing – review & editing, Validation, Supervision. **Qasim Rafiq:** Validation, Supervision, Formal analysis. **Nicolas Szita:** Writing – review & editing, Validation, Supervision, Funding acquisition, Formal analysis, Data curation, Conceptualization.

Declaration of Competing Interest

The authors declare the following financial interests/personal relationships which may be considered as potential competing interests: Nicolas Szita reports a relationship with Young Owl Microfluidics, Ltd that includes: equity or stocks. Nicolas Szita has patent #GB Patent Application GB0821636.8 and PCT/GB2009/002778 A issued to UCL Business. If there are other authors, they declare that they have no known competing financial interests or personal relationships that could have appeared to influence the work reported in this paper.

Acknowledgment

The authors gratefully acknowledge the Engineering and Physical Sciences Research Council (EPSRC) for the Future Targeted Healthcare

Manufacturing Hub hosted at University College London with UK university partners (Grant Reference: EP/P006485/1). The authors also gratefully acknowledge the funding from the EPSRC Centres for Doctoral Training (EP/L01520X/1, EP/S021868/1).

Appendix A. Supporting information

Supplementary data associated with this article can be found in the online version at doi:10.1016/j.bej.2026.110440.

Data availability

Data will be made available on request.

References

[1] C.H. June, R.S. O'Connor, O.U. Kawalekar, S. Ghassemi, M.C. Milone, CAR T cell immunotherapy for human cancer, Science 359 (2018) 1361–1365.
[2] A. Alnefaie, S. Albogami, Y. Asiri, T. Ahmad, S.S. Alotaibi, M.M. Al-Sanea, H. Althobaiti, Chimeric antigen receptor T-cells: an overview of concepts, applications, limitations, and proposed solutions, Front. Bioeng. Biotechnol. 10 (2022) 797440.
[3] P. Vormittag, R. Gunn, S. Ghorashian, F.S. Veraitch, A guide to manufacturing CAR T cell therapies, Curr. Opin. Biotechnol. 53 (2018) 164–181.
[4] M.C. Cavallo, M. Cavazza, F. Bonifazi, B. Casadei, I. Cutini, B. Tonietti, R. Saccardi, P.L. Zinzani, C. Jommi, Cost of implementing CAR-T activity and managing CAR-T patients: an exploratory study, BMC Health Serv. Res. 24 (2024) 12, https://doi.org/10.1186/s12913-023-10443-5.
[5] A.D. Kaiser, M. Assenmacher, B. Schröder, M. Meyer, R. Orentas, U. Bethke, B. Dropulic, Towards a commercial process for the manufacture of genetically modified T cells for therapy, Cancer Gene Ther. 22 (2015) 72–78.
[6] I. Ganeeva, E. Zmievskaya, A. Valiullina, A. Kudriaeva, R. Miftakhova, A. Rybalov, E. Bulatov, Recent advances in the development of bioreactors for manufacturing of adoptive cell immunotherapies, Bioeng. (Basel) 9 (2022) 808.
[7] T. Baudequin, R. Nyland, H. Ye, Objectives, benefits and challenges of bioreactor systems for the clinical-scale expansion of T lymphocyte cells, Biotechnol. Adv. 49 (2021) 107735.
[8] J.Aranda Hernandez, C. Heuer, J. Bahnemann, N. Szita, Microfluidic devices as process development tools for cellular therapy manufacturing, Adv. Biochem. Eng. Biotechnol. 179 (2022) 101–127.
[9] H. Kim, S. Kim, H. Lim, A.J. Chung, Expanding CAR-T cell immunotherapy horizons through microfluidics, Lab. Chip 24 (2024) 1088–1120.
[10] J. Darabi, C. Guo, On-chip magnetophoretic isolation of CD4 + T cells from blood, Biomicrofluidics 7 (2013) 54106.
[11] A.E. Rosenbach, P. Koria, J. Goverman, K.T. Kotz, A. Gupta, M. Yu, S.P. Fagan, D. Irimia, R.G. Tompkins, Microfluidics for T- lymphocyte cell separation and inflammation monitoring in burn patients, Clin. Transl. Sci. 4 (2011) 63–68.
[12] B.D. Plouffe, S.K. Murthy, Perspective on microfluidic cell separation: a solved problem? Anal. Chem. 86 (2014) 11481–11488.
[13] B. Kim, K.H. Kim, Y. Chang, S. Shin, E.-C. Shin, S. Choi, One-step microfluidic purification of white blood cells from whole blood for immunophenotyping, Anal. Chem. 91 (2019) 13230–13236.
[14] P.-L. Chiu, C.-H. Chang, Y.-L. Lin, P.-H. Tsou, B.-R. Li, Rapid and safe isolation of human peripheral blood B and T lymphocytes through spiral microfluidic channels, Sci. Rep. 9 (2019) 8145.
[15] H. Ide, W.V. Espulgar, M. Saito, T. Aoshi, S. Koyama, H. Takamatsu, E. Tamiya, Profiling T cell interaction and activation through microfluidics-assisted serial encounter with APCs, Sens. Actuators B Chem. 330 (2021), https://doi.org/10.1016/j.snb.2020.129306.
[16] A. Desalvo, F. Bateman, E. James, H. Morgan, T. Elliott, Time-resolved microwell cell-pairing array reveals multiple T cell activation profiles, Lab. Chip 20 (2020) 3772–3783.
[17] A.B.V. Quach, S.R. Little, S.C.C. Shih, Viral generation, packaging, and transduction on a digital microfluidic platform, Anal. Chem. 94 (2022) 4039–4047.
[18] C.A. Lissandrello, J.A. Santos, P. Hsi, M. Welch, V.L. Mott, E.S. Kim, J. Chesin, N. J. Haroutunian, A.G. Stoddard, A. Czarnecki, J.R. Coppeta, D.K. Freeman, D. A. Flusberg, J.L. Balestrini, V. Tandon, High-throughput continuous-flow microfluidic electroporation of mRNA into primary human T cells for applications in cellular therapy manufacturing, Sci. Rep. 10 (2020) 18045.
[19] R. Tran, D.R. Myers, G. Denning, J.E. Shields, A.M. Lytle, H. Alrowais, Y. Qiu, Y. Sakurai, W.C. Li, O. Brand, J.M. Le Doux, H.T. Spencer, C.B. Doering, W.A. Lam, Microfluidic transduction harnesses mass transport principles to enhance gene transfer efficiency, Mol. Ther. 25 (2017) 2372–2382.
[20] N. Moore, J.R. Chevillet, L.J. Healey, C. McBrine, D. Doty, J. Santos, B. Teece, J. Truslow, V. Mott, P. Hsi, V. Tandon, J.T. Borenstein, J. Balestrini, K. Kotz, A microfluidic device to enhance viral transduction efficiency during manufacture of engineered cellular therapies, Sci. Rep. 9 (2019) 15101.
[21] S.E. Ahmadi, R.M. Shabestari, A.A. Kojabad, M. Safa, A straightforward microfluidic-based approach toward optimizing transduction efficiency of HIV-1-derived lentiviral vectors in BCP-ALL cells, Biotechnol. Rep. (Amst.) 38 (2023) e00792.
[22] D.A. Farcas, C. Moore-Kelly, P. Stevenson, R.A.S. Raposo, M.P.C. Marques, N. Szita, Rethinking viral vector quantification: a microfluidic approach to standardised functional titre assays, Front. Bioeng. Biotechnol. 14 (2026) 1720882.
[23] A. Nikoniuk, K. Lilova, M. Thomas, N. Szita, The potential of microfluidic cell analysis in CAR T cell therapy manufacturing, Front. Bioeng. Biotechnol. 13 (2025) 1613836.
[24] K. Paterson, S. Paterson, T. Mulholland, S.B. Coffelt, M. Zagnoni, Assessment of CAR-T cell-mediated cytotoxicity in 3D microfluidic cancer co-culture models for combination therapy, IEEE Open. J. Eng. Med. Biol. 3 (2022) 86–95.
[25] W.-X. Sin, N.S. Jagannathan, D.B.L. Teo, F. Kairi, S.Y. Fong, J.H.L. Tan, D. Sandikin, K.-W. Cheung, Y.H. Luah, X. Wu, J.J. Raymond, F.L.W.I. Lim, Y. H. Lee, M.S.-F. Seng, S.Y. Soh, Q. Chen, R.J. Ram, L. Tucker-Kellogg, M. E. Birnbaum, A high-density microfluidic bioreactor for the automated manufacturing of CAR T cells, Nat. Biomed. Eng. 8 (2024) 1571–1591.
[26] Z. Wang, S.O. Kelley, Microfluidic technologies for enhancing the potency, predictability and affordability of adoptive cell therapies, Nat. Biomed. Eng. (2025), https://doi.org/10.1038/s41551-024-01315-2.
[27] L.N. Matos, M.S. Costa, M. Serra, M.H.G. Costa, Are we there yet? The road to faster and more efficient CAR T cell manufacturing, J. Biol. Eng. 20 (2026), https://doi.org/10.1186/s13036-026-00666-5.
[28] M. Reichen, R.J. Macown, N. Jaccard, A. Super, L. Ruban, L.D. Griffin, F. S. Veraitch, N. Szita, Microfabricated modular scale-down device for regenerative medicine process development, PLoS. One 7 (2012) e52246.
[29] A. Super, N. Jaccard, M.P.Cardoso Marques, R.J. Macown, L.D. Griffin, F. S. Veraitch, N. Szita, Real-time monitoring of specific oxygen uptake rates of embryonic stem cells in a microfluidic cell culture device, Biotechnol. J. 11 (2016) 1179–1189.
[30] W. Raimes, M. Rubi, A. Super, M.P.C. Marques, F. Veraitch, N. Szita, Transfection in perfused microfluidic cell culture devices: a case study, Process. Biochem. 59 (2017) 297–302.
[31] N. Abdolvand, R. Tostoes, W. Raimes, V. Kumar, N. Szita, F. Veraitch, Long-term retinal differentiation of human induced pluripotent stem cells in a continuously perfused microfluidic culture device, Biotechnol. J. 14 (2019), https://doi.org/10.1002/biot.201800323.
[32] N. Jaccard, R.J. Macown, A. Super, L.D. Griffin, F.S. Veraitch, N. Szita, Automated and online characterization of adherent cell culture growth in a microfabricated bioreactor, J. Lab. Autom. 19 (2014) 437–443.
[33] N. Jaccard, L.D. Griffin, A. Keser, R.J. Macown, A. Super, F.S. Veraitch, N. Szita, Automated method for the rapid and precise estimation of adherent cell culture characteristics from phase contrast microscopy images: automated method for adherent culture monitoring, Biotechnol. Bioeng. 111 (2014) 504–517.
[34] N. Jaccard, N. Szita, L.D. Griffin, Segmentation of phase contrast microscopy images based on multi-scale local Basic Image Features histograms, Comput. Methods Biomech. Biomed. Eng. Imaging Vis. 5 (2017) 359–367.
[35] M. Bajić, S. Khiawjan, S.T. Hilton, G.J. Lye, M.P.C. Marques, N. Szita, A paradigm shift for biocatalytic microreactors: decoupling application from reactor design, Biochem. Eng. J. 205 (2024) 109260.
[36] E. Costariol, M.C. Rotondi, A. Amini, C.J. Hewitt, A.W. Nienow, T.R.J. Heathman, Q.A. Rafiq, Demonstrating the manufacture of human CAR-T cells in an automated stirred-tank bioreactor, Biotechnol. J. 15 (2020) e2000177.
[37] B. Philip, E. Kokalaki, L. Mekkaoui, S. Thomas, K. Straathof, B. Flutter, V. Marin, T. Marafioti, R. Chakraverty, D. Linch, S.A. Quezada, K.S. Peggs, M. Pule, A highly compact epitope-based marker/suicide gene for easier and safer T-cell therapy, Blood 124 (2014) 1277–1287.
[38] P. Springuel, P. Silva Couto, D.J. Stibbs, M. Szelwicki, A. Frangleton, T. Schmidberger, A. George, F. Slingsby, N. Bevan, A. Ahmad, R. Legmann, N. Dianat, R. Ladi, J. Hengst, Q.A. Rafiq, Scalable CAR-T production in a 2-litre perfusion stirred-tank bioreactor with automated harvesting and scale-down model characterisation, Front. Bioeng. Biotechnol. 13 (2025) 1694134.
[39] P. Shah, I. Vedarethinam, D. Kwasny, L. Andresen, M. Dimaki, S. Skov, W. E. Svendsen, Microfluidic bioreactors for culture of non-adherent cells, Sens. Actuators B Chem. 156 (2011) 1002–1008.